

7. A. L. Casselman and J. B. Nasrallah, unpublished data.
8. J. A. Conner, P. Conner, M. E. Nasrallah, J. B. Nasrallah, *Plant Cell* **10**, 801 (1998).
9. cDNA libraries were constructed with the λ UNIZAP phagemid system (Stratagene). Hybridization conditions for RNA and DNA gel blots were as described [D. C. Boyes, C.-H. Chen, T. Tantikanjana, J. J. Esch, J. B. Nasrallah, *Genetics* **127**, 221 (1991)] except that washes (each 20 min at 65°C) were extended by using successively 2 \times SET, 0.5% SDS and 1 \times SET, 0.1% SDS and 0.2 \times SET, and 0.1% SDS, unless indicated otherwise.
10. The S_2S_6 F_2 population was derived from a cross between *B. oleracea* S_6S_6 and S_2S_2 homozygotes. The genotypes and SI phenotypes of 153 individual plants had been determined previously. Gel blot analysis of Hind III-digested genomic DNA revealed coinciding hybridization patterns for SLG_6^- and SCR_6^- -specific probes. All 116 plants hybridizing to SLG_6^- also hybridized to SCR_6^- , whereas all 37 plants devoid of SLG_6^- also lacked SCR_6^- . Similarly, 80 plants of an F_2 population segregating for S_6 and S_{13} were genotyped by hybridization of Hind III-digested genomic DNA with SLG_6^- and SLG_{13} -specific probes. Hybridization with an SCR_{13} -specific probe revealed that 34 SLG_{13} -containing plants contained SCR_{13} , in contrast to 46 plants lacking both SLG_{13} and SCR_{13} .
11. The *B. campestris* S_9 haplotype also appears to contain an SCR -related sequence [G. Suzuki *et al.*, *Genetics* **153**, 391 (1999)].
12. Polyadenylated RNA was analyzed as in (2, 9). Microspores were staged by DAPI (4',6'-diamidino-2-phenylindole) staining [S. Detchehare, P. Heizmann, C. Dumas, *J. Plant Physiol.* **135**, 129 (1989)] and purified as described [D. C. Boyes and J. B. Nasrallah, *Plant Cell* **7**, 1283 (1995)].
13. J. B. Nasrallah *et al.*, *Ann. Bot.*, in press.
14. As host for the transformation of the SCR_6 cDNA, we chose a *B. oleracea* S_2S_2 homozygote. Besides ease of transformation and regeneration, this strain is expected to have an endogenous SCR allele with only low sequence similarity to the transgene, which reduces the risk of homology-dependent gene silencing (Fig. 2A). The transformation construct contained the SCR_6 cDNA preceded by the SCR_8 1.3-kb upstream region and followed by the nos terminator. After introducing appropriate restriction sites by polymerase chain reaction followed by DNA sequence analysis, both SCR fragments were assembled as a transcriptional fusion in pCR2.1 (Invitrogen) and subcloned as a 1.7-kb Hind III-Sac I fragment into pCAMBIA1300 upstream of an Eco RI-Sac I nos promoter. After mobilization into *Agrobacterium tumefaciens* strain GV3101, the construct was used for transformation of flower stem disks of the *B. oleracea* S_2S_2 strain, as described [K. Toriyama, J. C. Stein, M. E. Nasrallah, J. B. Nasrallah, *Theor. Appl. Genet.* **81**, 769 (1991)], applying hygromycin selection. The independent origin of the transformants was verified by DNA gel blot analysis.
15. Pollen was manually transferred onto stigmas of open flowers. After 7 to 9 hours, pollen tube growth was observed by ultraviolet fluorescence microscopy [Y. O. Kho and J. Baer, *Euphytica* **17**, 298 (1968)].
16. Open reading frames encoded by the three cDNAs SCR_8 , SCR_{13} , and SCR_6 were identified on the basis of sequence similarity of the cysteine-rich reading frame, as well as the presence of stop codons upstream of the ATG initiation codon.
17. G. von Heijne, *Nucleic Acids Res.* **14**, 4683 (1986).
18. A. G. Stephenson *et al.*, *Plant J.* **12**, 1351 (1997).
19. J. Doughty *et al.*, *Plant Cell* **10**, 1333 (1998).
20. B. S. Stanchev, J. Doughty, C. P. Scutt, H. G. Dickinson, R. R. D. Croy, *Plant J.* **10**, 303 (1996).
21. W. F. Broekaert *et al.*, *Crit. Rev. Plant Sci.* **16**, 297 (1997); W. F. Broekaert, F. R. G. Terras, B. P. A. Cammue, R. W. Osborn, *Plant Physiol.* **108**, 1353 (1995); F. R. G. Terras *et al.*, *J. Biol. Chem.* **267**, 15301 (1992).
22. SI in *Brassica* is under sporophytic control, whereby pollen phenotype in S -locus heterozygotes is determined by the two S alleles carried by the diploid parent plant and not by the single S allele carried by the haploid pollen grain.
23. Supported by NIH grant GM57527, NSF grant IBN-9631921, and U.S. Department of Agriculture grant 98-358301-6072.

13 September 1999; accepted 26 October 1999

Molecular Architecture of the Rotary Motor in ATP Synthase

Daniela Stock,¹ Andrew G. W. Leslie,² John E. Walker^{1*}

Adenosine triphosphate (ATP) synthase contains a rotary motor involved in biological energy conversion. Its membrane-embedded F_0 sector has a rotation generator fueled by the proton-motive force, which provides the energy required for the synthesis of ATP by the F_1 domain. An electron density map obtained from crystals of a subcomplex of yeast mitochondrial ATP synthase shows a ring of 10 c subunits. Each c subunit forms an α -helical hairpin. The interhelical loops of six to seven of the c subunits are in close contact with the γ and δ subunits of the central stalk. The extensive contact between the c ring and the stalk suggests that they may rotate as an ensemble during catalysis.

ATP is the universal biological energy currency. ATP synthase produces ATP from adenosine diphosphate (ADP) and inorganic phosphate with the use of energy from a transmembrane proton-motive force generated by respiration or photosynthesis [for reviews, see (1–3)]. The enzyme consists of an extramembranous F_1 catalytic domain linked by means of a central stalk to an intrinsic membrane domain called F_0 . The globular F_1 domain is an assembly of five different subunits with the stoichiometry $\alpha_3\beta_3\gamma_1\delta_1\epsilon_1$. In the atomic structure of bovine F_1 , the α and β subunits are arranged alternately around a coiled coil of two antiparallel α helices in the γ subunit. The catalytic sites are in the β

subunits at the α/β subunit interface (4). The remainder of the γ subunit protrudes from the $\alpha_3\beta_3$ assembly and can be cross linked to the polar loop region of the c subunits in F_0 (5, 6). In mitochondria, the δ and ϵ subunits are associated with the γ subunit in the central stalk assembly (7–10), as are the bacterial and chloroplast ϵ subunits, the counterparts of mitochondrial δ . ATP-dependent rotation of γ and ϵ within an immobilized $\alpha_3\beta_3$ complex from the thermophilic bacterium *Bacillus* PS3 has been observed directly (11, 12). The rotation of the γ subunit in ATP synthase is thought to be generated by the passage of protons through F_0 . Because there is only one intrinsically asymmetric γ subunit, it interacts differently with each of the three catalytic β subunits in F_1 , endowing them with different nucleotide affinities (4). Rotation of the central stalk is accompanied by conformational changes in the β subunits, which cycle sequentially through structural states corresponding to low, medium, and high nu-

cleotide affinities. These three states are probably associated with release of product (ATP), binding of substrates (ADP and inorganic phosphate), and ATP formation, respectively. The cycle is known as the “binding change mechanism” of ATP synthesis (13). In eubacteria, the procedure is reversible, and hydrolysis of ATP in F_1 generates rotation of γ , resulting in the pumping of protons back across the membrane through F_0 (2).

In contrast to the detailed structural model established for most of the bovine F_1 domain (4, 14–16) and additional structural information in other species (17, 18), little is known about the structural details of F_0 . All species contain three common subunits known as a, b, and c. In *Escherichia coli*, the experimentally determined ratio of these subunits is $a_1b_2c_{9-11}$ (19, 20). Cross-linking and genetic experiments (21, 22), as well as evolutionary arguments (23), have been interpreted as showing the presence of 12 c subunits per F_0 . From biochemical studies and mutational analysis in bacteria (2, 24) and fungi (25), it is known that both a and c subunits contain functional groups that are essential for proton translocation through the membrane. A nuclear magnetic resonance (NMR) structure of a monomer of the *E. coli* c subunit in a chloroform:methanol:water mixture shows that the protein is folded into two α helices (presumed to be transmembrane in the intact enzyme), linked by a loop (presumed to be extramembranous) (26). The COOH-terminal α helix contains a conserved side chain carboxylate (Asp⁶¹ in *E. coli* and Glu⁵⁹ in *Saccharomyces cerevisiae*) essential for proton translocation (2). Models have been proposed in which the a and b subunits are on the

¹Medical Research Council Dunn Human Nutrition Unit, Hills Road, Cambridge CB2 2XY, UK. ²Medical Research Council Laboratory of Molecular Biology, Hills Road, Cambridge CB2 2QH, UK.

*To whom correspondence should be addressed. E-mail: walker@mrc-dunn.cam.ac.uk

outside of a multimeric ring of c subunits within the membrane, with the interface between a and c subunits providing the pathway for proton translocation (Fig. 1) (27–31). Protonation and deprotonation events in this interface have been proposed as part of a mechanism for generating conformational changes in F_1 (32), possibly through rotation of the c ring (33). Because the generation of each ATP requires rotation of the γ subunit through 120° , a link has been made between the number of protons that must be translocated per ATP synthesized [estimated to be three or four in different systems (34, 35)] and the number of c subunits in the ring. The required rotation of γ through 120° can be achieved with either 9 c subunits in the ring and 3 translocated protons or 12 c subunits in the ring and 4 translocated protons (36). It has also been proposed that a rotary mechanism would require a peripheral “stator” to counter the tendency of $\alpha_3\beta_3$ to follow the rotation of γ (36). It has been suggested that the b subunits of F_0 may form part of such a stator, and evidence from reconstitution and cross-linking studies provides support for this hypothesis (37, 38). A feature connecting the periphery of F_0 to F_1 (the peripheral stalk) that might represent the stator has been visualized by single-particle electron microscopy of ATP synthase from bacteria, chloroplasts, and mitochondria (39–41).

Structure analysis. In this study, we purified ATP synthase from *S. cerevisiae* mitochondria and carried out crystallization experiments (42). The enzyme from this source consists of at least 13 different types of subunits: the F_1 subunits α , β , γ , δ , and ϵ ; the F_0 subunits a, b, and c, plus f and d; OSCP and ATP8, which have homologs in other mitochondrial ATP synthases; and the unique yeast subunit h (43–46). Other possible yeast subunits have been discussed as being involved in dimer formation (47). According to analyses by SDS–polyacrylamide gel electrophoresis (SDS–PAGE), high-performance liquid chromatography (HPLC) analysis, and NH_2 -terminal sequencing, the purified complex used here for crystallization consists of subunits α , β , γ , δ , ϵ , b, OSCP, d, a, h, f, ATP8, and c (in diminishing apparent molecular weight order for F_1 and F_0 on SDS gels) and is similar to other preparations (46, 48, 49). Crystals were grown in the presence of both ADP and the nonhydrolyzable ATP analog 5'-adenylyl-imidodiphosphate (AMP-PNP) by the microbatch technique (50) with polyethylene glycol 6000 as precipitant (42). Subunits α , β , γ , δ , ϵ , and c were detected in the crystals by SDS–PAGE, and there was no evidence for the presence of the other subunits. It appears that they have dissociated from the complex during crystallization, leaving a subcomplex consisting of F_1 and 10 copies of subunit c. A similar F_1c_{10} complex

has been isolated previously from spinach chloroplasts (51).

The structure was solved by molecular replacement with the “stand-alone” version of the program AMoRe (52) with data from 15 to 5 Å resolution and the bovine F_1 –adenosine triphosphatase $C\alpha$ coordinates [Protein Data Bank (PDB) accession code 1bmf (4)] as a search model (Table 1). The complete bovine model, positioned according to the results of the molecular replacement, was used to calculate phases to 3.9 Å resolution. After solvent density modification with the program Solomon/CCP4 (53, 54) assuming a solvent content of 60%, the α helices of the c subunits and extensive additional density in the central stalk region could be seen in the electron density map (Fig. 2). Because of the limited resolution of the x-ray data, the side chain density is not clear, but the main chain density is generally unambiguous.

The crystal packing (Fig. 3) is typical for membrane proteins and belongs to neither of the types described previously (55). The main crystal contacts are between the bottom of a ring of 10 c subunits and the pseudo-three-fold top of an adjacent F_1 assembly. The hydrophobic external regions of the c oligomers, which are normally in contact with phospholipid, are not involved in any crystal contacts and are probably covered by unresolved molecules of detergent.

Molecular architecture of the F_1c_{10} complex. The α and β subunits (73 and 79% conserved, respectively, between cow and yeast) are well defined in the electron density and have similar conformations and nucleotide compositions to their bovine counterparts. The NH_2 - and COOH -terminal α helices of the γ subunit (40% sequence identity to the bovine subunit) extend ~ 25 Å farther than in the bovine model toward the c subunits, where they make a sharp bend. In the

bovine F_1 structure, this part of the γ subunit and also subunits δ and ϵ were disordered. There is additional density adjacent to the lower segment of the NH_2 -terminal α helix of the γ subunit that extends over the c subunits (Fig. 2B), which can be interpreted with the crystal structure of the *E. coli* ϵ subunit (26% sequence identity to the yeast δ subunit) (56) (PDB accession code 1aqt). The 10 strands of the β barrel are visible in the yeast electron density, with β strand 4 and the following loop (residues 31 to 39 in *E. coli* numbering) packing against the c subunits and β strands 5, 8, 9, and the loop between β strands 1 and 2 (residues 39 to 42, 68 to 73, 74 to 79, and 9 to 14, respectively) in contact with the γ subunit. The lower α helix (COOH -terminal) lies about 5 Å above the c subunits, and the upper α helix is closer to the $\alpha_3\beta_3$ subcomplex, extending into the solvent. This interpretation of the yeast electron density is in general agreement with a previous model of the *E. coli* F_1c complex (56) and with cross-linking studies (57), although it cannot explain cross linking between the *E. coli* ϵ subunit and the DELSEED region of a β subunit (9).

The electron densities of individual c subunits show that they consist of two α helices, linked by a loop. There is no interpretable side chain density, and the density could not be improved by modeling the subunits as polyalanine or by averaging. Therefore, it is not yet possible to build an unambiguous atomic model. The electron density is consistent with the NMR structure of the *E. coli* monomer determined in a chloroform:methanol:water mixture (26) (PDB accession code 1a91). Although the overall shape of the *E. coli* and the yeast c monomers is similar, the *E. coli* structure is not a perfect match to the yeast density (Fig. 2B). This could be due to the low sequence conservation (23% identity)

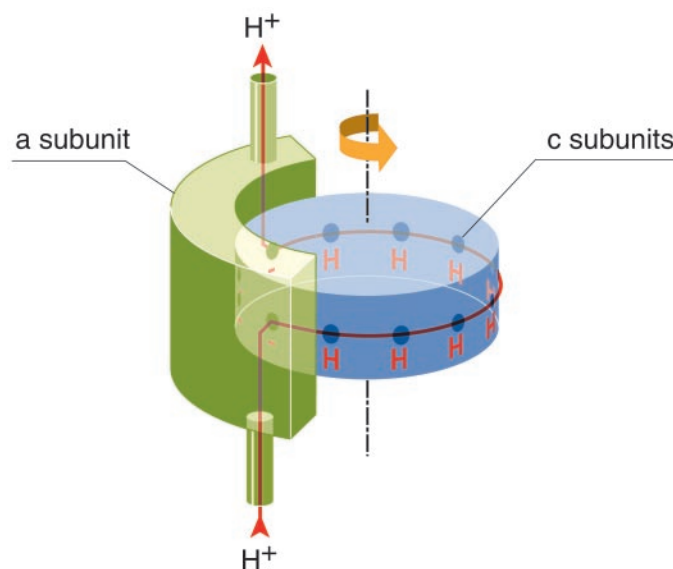


Fig. 1. Hypothetical model for the generation of rotation by proton transport through the F_0 domain of ATP synthase [according to Junge (33)]. The central cylinder (blue) consists of c subunits; the external part (green) corresponds to a single a subunit. The red line indicates the proton path. [Reproduced with kind permission of the Swedish Academy of Sciences.]

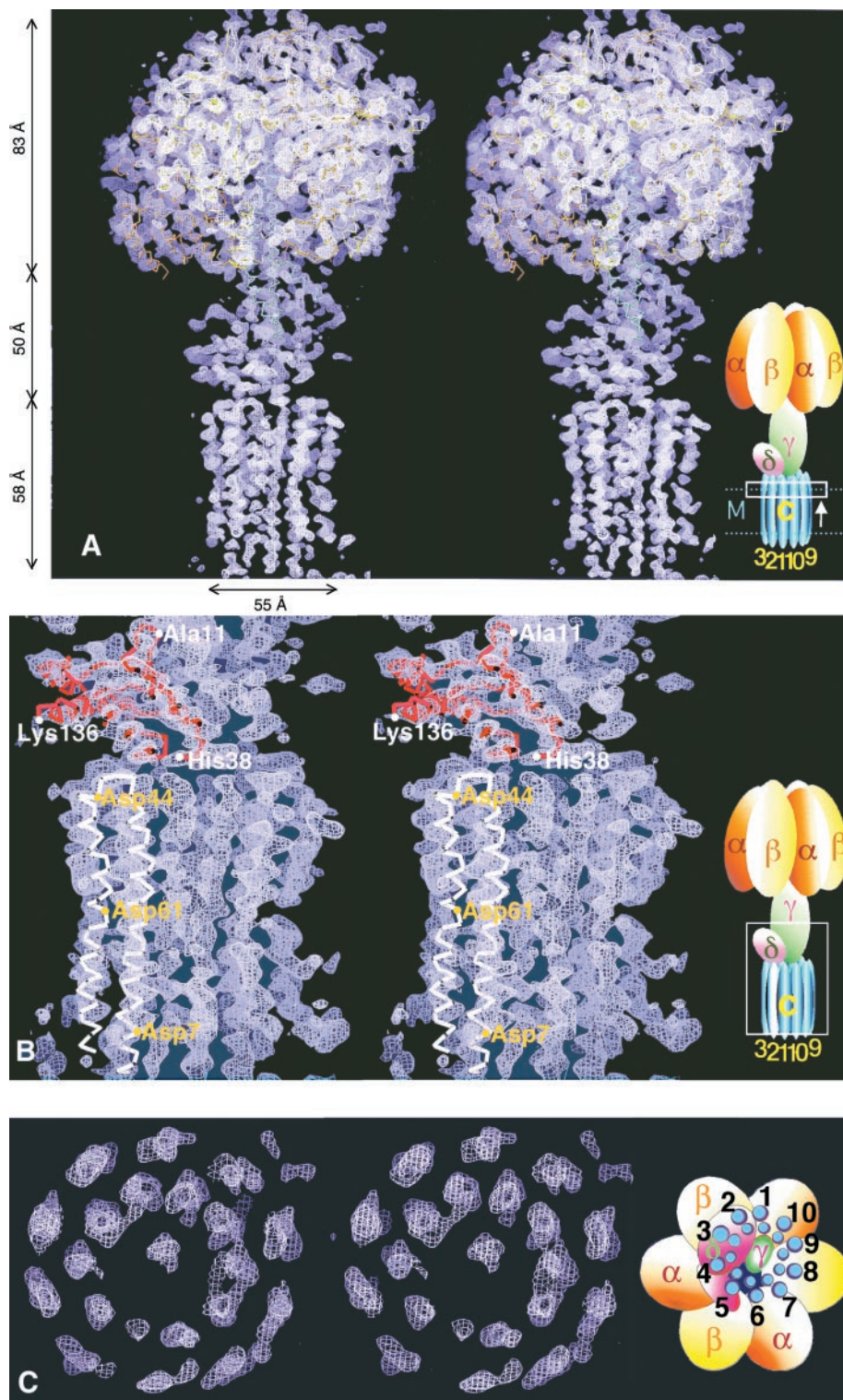
RESEARCH ARTICLES

between the two species, or it could, at least in part, arise from the contacts between neighboring protomers. The 10 *c* protomers are packed tightly against each other, forming two rings of single α helices (see Fig. 2C). The outer α helices are kinked in the middle, making the cylindrical outer surface of the oligomer slightly concave. Despite the absence of clear side chain density, it is possible to assign the α

helices forming the inner and outer rings to the NH₂-terminal and COOH-terminal regions, respectively, as follows. Cysteine residues introduced at positions 40, 42, and 44 of the *E. coli* *c* subunit (equivalent to 38, 40, and 42 in yeast) can be cross linked to the ϵ subunit in the *E. coli* enzyme and are therefore thought to lie in the polar loop between the two α helices (57). The density for the inner α helix is 58 Å long and

would accommodate 39 residues in an α -helical conformation, consistent with residues 40 to 44 forming the polar loop. The density for the outer α helix is 47 Å long. This would accommodate 31 residues in an α -helical conformation, which is in excellent agreement with the total of 76 residues in the yeast *c* subunit. The kink of about 23° in the COOH-terminal α helix is around Gly⁶² (equivalent to Pro⁶⁴ in *E.*

Fig. 2. Stereo views of an electron density map of the yeast F_1c_{10} complex. The solvent flattened map was calculated at 3.9 Å resolution and contoured at 1.5 σ . (A) Side view containing the bovine F_1 C α model (with α in orange, β in yellow, and γ in green). The density of symmetry-related molecules in the crystal is masked out. The inset indicates the location of the subunits within the complex. The location of the section shown in (C) is indicated by the white box; the direction of the view is indicated by the arrow. The presumed membrane region (M) (2) is marked by the two dotted lines. The *c* subunits are numbered 3, 2, 1, 10, and 9 (the best ordered *c* subunit was chosen as number 1). The overall height of the complex is ~190 Å, of which the $\alpha_3\beta_3$ subcomplex accounts for 83 Å, the stalk for 50 Å, and the *c* subunits for 58 Å. (B) Enlarged view of the δ/γ -*c* contact region with the model (and numbering) of the *E. coli* ϵ subunit (in red) and the *E. coli* *c* subunit (in white) fitted into the density, contoured at 1.0 σ . The white box in the inset indicates the location of the displayed section within the complex. (C) End-on view of the density of the *c* ring. The inset shows the location of the α , β , γ , and δ subunits in relation to the *c* subunits. The helices of the *c* subunit are drawn as blue circles, the larger outer circles accounting for the larger side chains in the COOH-terminal helix. The outer diameter of the *c* ring is 55 Å (top) to 42 Å (equator) to 45 Å (bottom), and the inner diameter is 27 Å (top) to 17 Å (equator) to 22 Å (bottom). The dimensions exclude consideration of unresolved regions of density, including amino acid side chains and detergent or lipid molecules. The two regions of density near subunit 10 are not extensive and are likely to be noise.



coli). This arrangement would also place the glycine/alanine-rich NH₂-terminal α helix in the inner ring and accommodate the larger side chains of the COOH-terminal α helix in the outer ring. Because of the lack of side chain density, the conserved carboxylate (Glu⁵⁹) cannot be placed with certainty, but it would lie about halfway along the outer COOH-terminal α helix. The resulting model shares many features in common with that proposed for the *E. coli* ring of c subunits (58), except that the latter contains 12 rather than 10 copies. It differs from an alternative model (59, 60), which placed the NH₂-terminal helices on the outside. A model for the c subunit of the sodium-driven enzyme from *Propionigenium modestum* based on NMR data consists of four distinct α -helical segments with the conserved carboxylate located near the cytoplasmic membrane surface (61). There is no evidence for four distinct α helices in the yeast density, and the conserved carboxylate would appear to lie more centrally within the membrane, although the position of the

membrane boundary cannot be defined with certainty.

The 10 c subunits form an almost symmetrical ring, although the density for subunits 6, 7, and 8 is weaker, as seen from the asymmetrical appearance of the electron density (Fig. 2C). The central cavity of the c oligomer contains a region of elongated electron density, which is stronger in the upper and lower thirds of the cylinder than in the center (Fig. 2C). The origin of this density is not clear, but the need to maintain a semipermeable membrane *in vivo* suggests that the cavity might be filled with phospholipid.

The polar loop regions of five of the c subunits (c1 to c5) are covered by the δ subunit (Fig. 2B). Two loops (c2 and c3) are in intimate contact, probably involving hydrogen bonds between pairs of main chain atoms, and another three (c1, c4, and c5) could form side chain contacts to either the β barrel of the δ subunit or the lower of its two α helices. The γ subunit probably makes side chain contacts to one or

two further c subunits (c9 and c10) and to one subunit (c1) that is also in contact with the β barrel of the δ subunit. Therefore, six or seven consecutive c subunits or about two-thirds of the top surface of the ring are in contact with the foot of the stalk. These c subunits are much better defined in the electron density than the exposed ones, in which the density is weaker and discontinuous. The 62 residues of the yeast ϵ subunit could not be assigned unambiguously to the density, and about 100 residues of the γ subunit remain unassigned, although there is extensive uninterpreted electron density both on top of the δ subunit and next to the COOH-terminal α helix of γ .

The extent of the interface between the c subunits and the γ and ϵ subunits apparent in the electron density map of the yeast F₁c₁₀ oligomer supports the hypothesis that the complex consisting of the γ , δ (*E. coli* ϵ), ϵ , and c subunits rotates as an ensemble during catalysis, but other interpretations are still possible.

Functional implications of the c ring stoichiometry. An unexpected feature of the electron density map is that the ring of c subunits contains 10 protomers and not, as widely anticipated, 12 (21–23, 58–60). At this stage of the analysis, it is possible that some c subunits have been lost from the ring during crystallization. However, the extent of the interaction between adjacent c subunits within the ring makes this unlikely, particularly as there is no evidence to suggest a strong association between subunit c and any of the other components of F₀. In addition, it is likely that the crystal contact between the ring of c subunits and the pseudo-three-fold F₁ domain would have selected for a population of complexes with 12 c subunits, if present. In consequence, the three-fold symmetry of the F₁ sector and the 10-fold symmetry of the c ring within one complex do not match. The principle of symmetry mismatch in

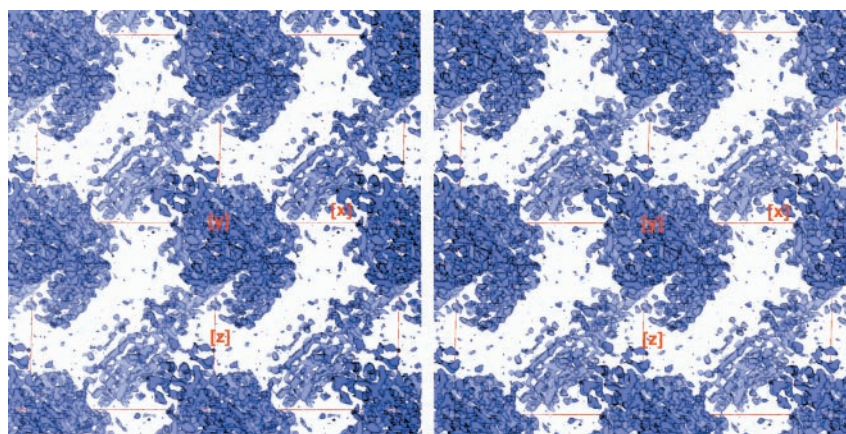


Fig. 3. Stereo view of the crystal packing of the yeast F₁c₁₀ complex. A 45 Å thick section through the crystal perpendicular to the crystallographic y axis is shown. The electron density is contoured at 1.2 σ . The red lines mark the x and z axes of the crystal lattice. All figures were prepared with the program MAIN (72).

Table 1. Statistics of data collection and structure determination. For data collection, the crystals were harvested in a buffer containing 20% glycerol as cryo-protectant and then frozen rapidly in liquid nitrogen. The crystals are small (up to 150 μ m in the largest dimension) and diffract x-rays weakly. They belong to the monoclinic space group P2₁ with unit cell dimensions a = 135.9 Å, b = 175.3 Å, c = 139.2 Å, and β = 91.6°. Assuming one F₁c₁₀

complex with 453.2 kD per asymmetric unit, the estimated solvent content is 66%. A data set was collected to 3.6 Å resolution at beamline ID02B (λ = 0.99 Å), at the ESRF, Grenoble, France, with a Mar Research image plate detector (1600 pixel mode). The data were processed with MOSFLM (73) and SCALA/CCP4 (54). Because of anisotropic diffraction and slight radiation damage, the final data set was restricted to 3.9 Å resolution.

Resolution shell (Å)	12.33	8.72	7.12	6.17	5.52	5.03	4.66	4.36	4.11	3.90	Overall (15–3.9)
Number of observations	1343	3207	4159	4934	5600	6229	6765	7312	7756	8288	55593
Completeness (%)	69.8	92.2	92.8	93.3	93.5	94.1	94.1	94.8	94.5	95.5	93.3
R _{merge} * (%)	5.8	5.6	6.7	8.7	10.4	11.9	12.0	14.3	22.1	37.2	10.0
I/ σ	7.2	6.6	7.4	6.7	6.3	5.5	5.4	4.7	3.3	1.3	4.0
Resolution range	15.0–5.0 Å										
Molecular replacement correlation coefficient	54.1 (44.0) [†]										
Molecular replacement R factor (%) [‡]	46.7 (50.6)										

*R_{merge}: $\sum_h \sum_i [|I_{(h,i)} - \langle I_{(h)} \rangle|] / \sum_h \sum_i I_{(h,i)}$, where $I_{(h,i)}$ is the intensity value of the i th measurement of h and $\langle I_{(h)} \rangle$ is the corresponding mean value of h for all i measurements of h . The summation runs over all measurements. [†]Values for the second highest solution are given in parentheses. [‡]R factor: $\sum |F_{\text{obs}} - F_{\text{calc}}| / \sum |F_{\text{obs}}|$, where F_{obs} and F_{calc} are the observed and calculated structure factor amplitudes, respectively.

molecular rotary engines has been discussed in relation to the DNA translocating machinery of bacteriophages (62, 63). During phage assembly, DNA is injected through the sixfold symmetrical tail into its head (fivefold symmetry axis of an icosahedron). The dodecameric head-tail connector is believed to rotate with respect to the head during DNA packaging (64). The symmetry mismatch between the head and the connector is thought to facilitate rotation by avoiding deeper energy minima that would accompany matching symmetries. Symmetry mismatch also appears to be important in the bacterial flagellar motor, which, similar to ATP synthase, is driven by the proton-motive force (65). A further example of symmetry mismatch is found in some ATP-dependent proteases (66), where a rotational mechanism has been suggested to contribute to protein unfolding. The arrangement of the components of the molecular motor in ATP synthase is rather different than that in either the bacteriophage or ATP-dependent proteases. In the latter cases, there are direct interactions between two rings of subunits with different symmetries. In the ATP synthase, there are two quite distinct regions of interaction. The first, in F_1 , involves the γ subunit and the $\alpha_3\beta_3$ subcomplex, whereas the second, in F_0 , involves the ring of c subunits and the a subunit.

The number of c subunits in the ring has profound implications for the number of protons translocated by F_0 for each ATP molecule synthesized in F_1 . Each ATP synthetic event requires that the γ subunit rotates through 120° . This rotation is generated in F_0 either by rotation of the c ring with γ (as the F_1c_{10} structure appears to indicate) or by some other mechanism in which the c subunits impart rotation to γ without themselves rotating. A c stoichiometry of 9 or 12 has been considered to require translocation of three or four protons per ATP synthesized to impart a 120° rotation to the c ring (see Fig. 1). A ring with 10 c subunits in it suggests that the H^+ /ATP ratio is probably nonintegral and that its value lies between 3 and 4. Many of the experimentally measured H^+ /ATP ratios lie in this range (34, 35).

Assuming that the c ring and γ subunit rotate as an ensemble, a nonintegral H^+ /ATP ratio also makes it more likely that there is some degree of elasticity in the γ subunit itself, so that the stepping of the c ring (10 steps per rotation) can be matched to the stepping in F_1 (three steps per rotation). Elasticity in the γ subunit is an explicit feature of two models for ATP synthase (67, 68), whereas in a third model (69) it is not required.

It has been suggested that the number of c subunits in *E. coli* varies depending on the carbon source (70, 71). More c subunits appear to be assembled into the complex if cells are grown in glucose than with succinate. Therefore, in the latter case, the c ring would be

smaller with an accompanying reduced gearing ratio. Changing gears and therefore the membrane potential required for ATP synthesis could be a regulatory mechanism. A variable number of c subunits could also explain the observation that covalently linked trimers of *E. coli* c subunit can form an active complex (22).

The electron density shown here provides direct proof that c protomers form a ring that is in close contact with the γ and δ subunits. Our interpretation is consistent with previous ones, in which subunits γ , δ , and ϵ form a rotating ensemble. It strongly supports the idea that the c oligomer is part of a rotary motor, converting electrochemical energy into chemical energy stored in ATP. To understand the mechanism of the generation of rotation, it will be necessary to establish the nature of the interaction between the c subunit oligomer found here and the remaining subunits in F_0 .

References and Notes

- P. D. Boyer, *Annu. Rev. Biochem.* **66**, 717 (1997).
- R. H. Fillingame, *Bacteria* **12**, 345 (1990).
- A. E. Senior, *Annu. Rev. Biophys. Biophys. Chem.* **19**, 7 (1990).
- J. P. Abrahams, A. G. W. Leslie, R. Lutter, J. E. Walker, *Nature* **370**, 621 (1994).
- S. D. Watts, C. L. Tang, R. A. Capaldi, *J. Biol. Chem.* **271**, 28341 (1996).
- S. D. Watts, Y. Zhang, R. H. Fillingame, R. A. Capaldi, *FEBS Lett.* **368**, 235 (1995).
- K. Sawada, H. Watanabe, C. Moritani-Otsuka, H. Kanazawa, *Arch. Biochem. Biophys.* **348**, 183 (1997).
- G. B. Cox et al., *J. Mol. Biol.* **229**, 1159 (1993).
- R. Aggeler, M. A. Haughton, R. A. Capaldi, *J. Biol. Chem.* **270**, 9185 (1995).
- G. L. Orriss et al., *Biochem. J.* **314**, 695 (1996).
- H. Noji, R. Yasuda, M. Yoshida, K. Kinoshita, *Nature* **386**, 299 (1997).
- Y. Kato-Yamada, H. Noji, R. Yasuda, K. Kinoshita, M. Yoshida, *J. Biol. Chem.* **273**, 19375 (1998).
- P. D. Boyer, *Biochim. Biophys. Acta* **1140**, 215 (1993).
- J. P. Abrahams et al., *Proc. Natl. Acad. Sci. U.S.A.* **93**, 9420 (1996).
- M. Van Raaij, J. P. Abrahams, A. G. W. Leslie, J. E. Walker, *Proc. Natl. Acad. Sci. U.S.A.* **93**, 6913 (1996).
- G. L. Orriss, A. G. W. Leslie, K. Braig, J. E. Walker, *Structure* **6**, 831 (1998).
- M. A. Bianchet, J. Hüllihen, P. L. Pedersen, L. M. Amzel, *Proc. Natl. Acad. Sci. U.S.A.* **95**, 11065 (1998).
- Y. Shirakihara et al., *Structure* **5**, 825 (1997).
- D. L. Foster and R. H. Fillingame, *J. Biol. Chem.* **257**, 2009 (1982).
- R. H. Fillingame, P. C. Jones, W. Jiang, F. I. Valiyaveetil, O. Y. Dmitriev, *Biochim. Biophys. Acta* **1365**, 135 (1998).
- P. C. Jones, W. Jiang, R. H. Fillingame, *J. Biol. Chem.* **273**, 17178 (1998).
- P. C. Jones and R. H. Fillingame, *J. Biol. Chem.* **273**, 29701 (1998).
- C. Ruppert et al., *J. Biol. Chem.* **274**, 25281 (1999).
- F. I. Valiyaveetil and R. H. Fillingame, *J. Biol. Chem.* **272**, 32635 (1997).
- R. J. Devenish et al., *Ann. N.Y. Acad. Sci.* **671**, 403 (1992).
- M. E. Girvin, V. K. Rastogi, F. Abildgaard, J. L. Markley, R. H. Fillingame, *Biochemistry* **37**, 8817 (1998).
- W. P. Jiang and R. H. Fillingame, *Proc. Natl. Acad. Sci. U.S.A.* **95**, 6607 (1998).
- G. Kaim, U. Matthey, P. Dimroth, *EMBO J.* **17**, 688 (1998).
- S. B. Vik, A. R. Patterson, B. J. Antonio, *J. Biol. Chem.* **273**, 16229 (1998).
- K. Takeyasu et al., *FEBS Lett.* **392**, 110 (1996).
- S. Singh, P. Turina, C. J. Bustamante, D. J. Keller, R. Capaldi, *FEBS Lett.* **397**, 30 (1996).
- R. H. Fillingame, *Biochim. Biophys. Acta* **1101**, 240 (1992).
- W. Junge, H. Lill, S. Engelbrecht, *Trends Biochem. Sci.* **22**, 420 (1997).
- D. G. Nicholls and S. J. Ferguson, *Bioenergetics 2* (Academic Press, London, 1992).
- S. Berry and B. Rumberg, *Biochim. Biophys. Acta* **1276**, 51 (1996).
- J. E. Walker, *Angew. Chem.* **37**, 2308 (1998).
- I. R. Collinson et al., *J. Mol. Biol.* **242**, 408 (1994).
- S. Engelbrecht and W. Junge, *FEBS Lett.* **414**, 485 (1997).
- S. Wilkens and R. A. Capaldi, *Nature* **393**, 29 (1998).
- B. Böttcher, L. Schwarz, P. Gräber, *J. Mol. Biol.* **281**, 757 (1998).
- S. Karrasch and J. E. Walker, *J. Mol. Biol.* **290**, 379 (1999).
- A portion (100 g) of a block of commercial baker's yeast (*S. cerevisiae*) was suspended in 250 ml of buffer containing 20 mM tris (pH 8.0), 1 mM ethylenediaminetetraacetic acid, 1 mM dithiothreitol (DTT), 0.5 M D-sorbitol, 0.001% phenylmethylsulfonyl fluoride (PMSF), and 2.5 ml of protease inhibitor cocktail (Sigma, catalog number P-8215). Cells were broken in a bead beater (Biospec) by four treatments each of 1-min duration. Cell debris was removed by centrifugation several times at 1500g, and mitochondria were collected by centrifugation for 1 hour at 24,000g. The mitochondrial pellet was resuspended in 250 ml of buffer A [20 mM tris (pH 8.0), 50 mM trehalose, 10% glycerol, 2 mM magnesium chloride, 1 mM ethylenediaminetetraacetic acid, 0.001% PMSF, 0.1% dodecylmaltoside, 1 mM DTT, and 0.02% sodium azide]. Protease inhibitor cocktail (2.5 ml, Sigma), deoxyribonuclease I (100 mg, Sigma), and dodecylmaltoside (2.5 g, Sigma) were added. Insoluble material was removed by centrifugation (1 hour, 142,000g), and the supernatant was applied to a 70-ml Q-Sepharose column. ATP synthase was eluted in a step gradient from 140 to 200 mM sodium chloride in buffer A. The concentrated enzyme was applied to a Sephacryl 300 column (320 ml, equilibrated in buffer A, 100 mM sodium chloride). Fractions containing ATP synthase (~20 mg typical yield) were pooled and concentrated to a protein concentration of 10 mg/ml. Disruption of the cells and all steps of the purification were performed at 4°C. Crystals were grown at 4°C under paraffin oil by the microbatch method by adding 2 μ l of buffer containing 0.1 M tris (pH 8.0), 12% polyethylene glycol 6000, 150 mM sodium chloride, 1 mM AMP-PNP, 40 μ M ADP, 1 mM DTT, and 0.02% sodium azide to 2 μ l of protein solution.
- M. Bateson, R. J. Devenish, P. Nagley, M. Prescott, *J. Biol. Chem.* **274**, 7462 (1999).
- M. Prescott et al., *FEBS Lett.* **411**, 97 (1997).
- C. Spannagel, J. Vaillier, G. Arselin, P. V. Graves, J. Velours, *Eur. J. Biochem.* **247**, 1111 (1997).
- G. Arselin, J. Vaillier, P. V. Graves, J. Velours, *J. Biol. Chem.* **271**, 20284 (1996).
- I. Arnold, K. Pfeiffer, W. Neupert, R. A. Stuart, H. Schagger, *EMBO J.* **17**, 7170 (1998).
- R. H. P. Law, S. Manon, R. J. Devenish, P. Nagley, *Methods Enzymol.* **260**, 133 (1995).
- M. Bateson, R. J. Devenish, P. Nagley, M. Prescott, *Anal. Biochem.* **238**, 14 (1996).
- N. E. Chayen, P. D. S. Stewart, D. M. Blow, *J. Crystal Growth* **122**, 176 (1992).
- C. M. Wetzel and R. E. McCarty, *Plant Physiol.* **102**, 241 (1993).
- J. Navaza, *Acta Crystallogr. Sect. A* **50**, 157 (1994).
- J. P. Abrahams and A. G. W. Leslie, *Acta Crystallogr. Sect. D* **52**, 30 (1996).
- Collaborative Computational Project Number 4, *Acta Crystallogr. Sect. D* **50**, 760 (1994).
- H. Michel, *Trends Biochem. Sci.* **8**, 56 (1983).
- U. Uhlin, G. B. Cox, J. M. Guss, *Structure* **5**, 1219 (1997).
- J. Hermolin, O. Y. Dmitriev, Y. Zhang, R. H. Fillingame, *J. Biol. Chem.* **274**, 17011 (1999).
- O. Y. Dmitriev, P. C. Jones, R. H. Fillingame, *Proc. Natl. Acad. Sci. U.S.A.* **96**, 7785 (1999).
- G. Groth and J. E. Walker, *FEBS Lett.* **410**, 117 (1997).
- G. Groth, Y. Tilg, K. Schirwitz, *J. Mol. Biol.* **281**, 49 (1998).
- U. Matthey, G. Kaim, D. Braun, K. Wüthrich, P. Dimroth, *Eur. J. Biochem.* **261**, 459 (1999).

62. R. W. Hendrix, *Proc. Natl. Acad. Sci. U.S.A.* **75**, 4779 (1978).
63. ———, *Cell* **94**, 147 (1998).
64. J. M. Valpuesta, J. J. Fernandez, J. M. Carazo, J. L. Carrascosa, *Structure* **7**, 289 (1999).
65. D. R. Thomas, D. G. Morgan, D. J. DeRosier, *Proc. Natl. Acad. Sci. U.S.A.* **96**, 10134 (1999).
66. F. Beuron *et al.*, *J. Struct. Biol.* **123**, 248 (1998).
67. D. A. Cherepanov, A. Y. Mulikdjanian, W. Junge, *FEBS Lett.* **449**, 1 (1999).
68. O. Pänke and B. Rumberg, *Biochim. Biophys. Acta* **1412**, 118 (1999).
69. T. Elston, H. Y. Wang, G. Oster, *Nature* **391**, 510 (1998).
70. R. A. Schemidt, J. Qu, J. R. Williams, W. S. A. Brusilow, *J. Bacteriol.* **180**, 3205 (1998).
71. R. A. Schemidt, D. K. W. Hsu, G. Deckers-Hebestreit, K. Altendorf, W. S. A. Brusilow, *Arch. Biochem. Biophys.* **323**, 423 (1995).
72. D. Turk, thesis, Technische Universität München, Munich, Germany (1992).
73. A. G. W. Leslie, *Joint CCP4 and ESF-EACMB Newsletter Protein Crystallography* (Daresbury Laboratory, Warrington, UK, 1992).

74. We thank R. Henderson for comments on the manuscript, S. Y. Peak-Chew and I. M. Fearnley for NH₂-terminal sequencing and HPLC analysis, and the staff of beamline ID02B at European Synchrotron Radiation Facility (ESRF), Grenoble, for help with data collection. D.S. was supported during part of this work by an European Molecular Biology Organization Fellowship. The coordinates of an unrefined C α model based on the bovine F₁ (1bmf) and the *E. coli* c (1a91) and ϵ (1aqt) coordinates have been deposited in the Protein Data Bank (accession code 1qo1).

27 September 1999; accepted 1 November 1999

REPORTS

First-Principles Determination of Elastic Anisotropy and Wave Velocities of MgO at Lower Mantle Conditions

B. B. Karki,¹ R. M. Wentzcovitch,¹ S. de Gironcoli,² S. Baroni²

The individual elastic constants of magnesium oxide (MgO) have been determined throughout Earth's lower mantle (LM) pressure-temperature regime with density functional perturbation theory. It is shown that temperature effects on seismic observables (density, velocities, and anisotropy) are monotonically suppressed with increasing pressure. Therefore, at realistic LM conditions, the isotropic wave velocities of MgO remain comparable to seismic velocities, as previously noticed in athermal high-pressure calculations. Also, the predicted strong pressure-induced anisotropy is preserved toward the bottom of the LM, so lattice-preferred orientations in MgO may contribute substantially to the observed seismic anisotropy in the D'' layer.

The last few years have seen rapid progress in our understanding of the behavior of the major mineral phases of Earth's mantle. Recent advances in theory and computation have made it possible to predict from first principles the structural and elastic properties of these materials throughout the entire pressure regime of the mantle (1). Experimental studies are now also possible over considerable ranges of pressure (P) and temperature (T) (2–5). However, the challenge of experimentally or theoretically determining the mineral properties at simultaneous P and T conditions of geophysical magnitudes is still enormous. Such studies will provide the basis for an improved analytical treatment of fundamental issues in Earth sciences, such as (i) constraining the mineralogy of the deep interior by directly comparing the seismic velocities (6) with predicted velocities for various mineral aggregates; (ii) describing Earth's thermal state by distinguishing thermal versus compositional effects on wave velocities; and (iii) understanding the sources of seismic anisotropies such as

those observed at D'' (7). It has been suggested that mantle flow and the accompanying stress field (in the vicinity of boundaries) could align crystalline axes along preferred directions and create anisotropic fabrics carrying the signature of the flow pattern (8).

The possibility of calculating with high accuracy and computational efficiency the entire vibrational spectrum of a crystal with the use of density functional perturbation theory (9) allows us to determine from first principles the crystal free energy, $F(V,T)$, from which we can extract all measurable thermodynamic quantities for the mineral, including the elastic moduli. Here we chose to start with the pressure and temperature dependence of the elastic constants of MgO (10), which exists as (Mg_{0.8}Fe_{0.2})O-magnesiowüstite in the lower mantle (LM) with 20 to 30% abundance according to a typical pyrolytic model (11). A previous first principles study of high-pressure (athermal) elasticity (12) showed that MgO is strongly anisotropic at D'' pressures (125 to 135 GPa) and its wave velocities are higher than seismic velocities throughout the LM pressure regime (23 to 135 GPa). Although T -induced effects at ambient P or so are known to be substantial and to counteract those of pressure

(4, 5), the effects at high P 's are unknown.

The results presented below were obtained within the quasi-harmonic approximation (QHA). It is a good approximation for MgO at ambient P up to ≈ 1000 K (13), as can be seen by comparing calculated and measured thermal expansivities, α (14) (see Fig. 1). The deviation of α from linearity at ambient P and high T 's is related to the inadequacy of the QHA and can be traced back to the behavior of the mode Grüneisen parameters with volume (15). The agreement with experiments at about 1800 K and 180 GPa (16), as well as the predicted linear behavior at high P 's and T 's, indicate that the QHA is valid at geophysically relevant conditions.

The adiabatic elastic constants (c_{11} , c_{12} , and c_{44}) were obtained as a function of P and T to 150 GPa and 3000 K, respectively, by calculating the free energies for the strained lattices (17). The predicted ambient values and their initial pressure (at 300 K) and temperature (at 0 GPa) dependencies agree with

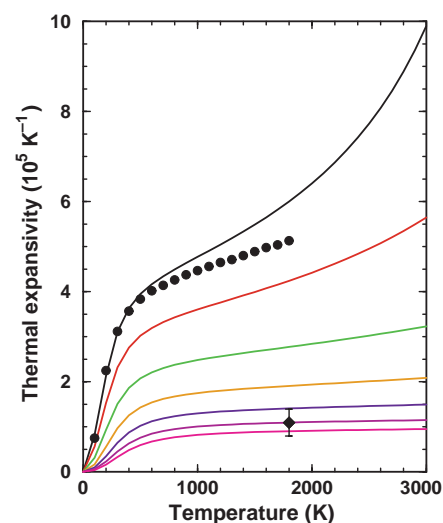


Fig. 1. Temperature dependence of thermal expansivity of MgO along several isobars at 0, 10, 30, 60, 100, 150, and 200 GPa (solid lines from top to bottom). The experimental data at zero pressure (14) are denoted by circles. The average value of α between 300 and ~ 3300 K at 169 to 196 GPa derived from shock-wave experiments (16) is denoted by the diamond.

¹Department of Chemical Engineering and Materials Science, Minnesota Supercomputing Institute, University of Minnesota, Minneapolis, MN 55455, USA.

²Scuola Internazionale Superiore di Studi Avanzati (SISSA), I-34014 Trieste, Italy.